Design of a high voltage dc-dc converter for automotive applications using 650 V GaN devices

Ilias Chorfi[1,2,3], Corinne Alonso[2], Romain Montheard[3], Thierry Sutto[1]
[1]STMicroelectronics, Automotive & Discrete Group (ADG). Labège, France
[2]LAAS-CNRS, Université de Toulouse, CNRS, UPS. Toulouse, France
[3]Commissariat à l'énergie atomique et aux énergies alternatives (CEA). Labège, France.

Abstract – This paper discusses a bidirectional three-level Dual Active Half Bridge (DAHB) DC-DC converter for high voltage on-board charger (OBC) application using 650V GaN on Silicon FETs. The half bridge configuration on each side of the transformer helps reducing the component count and increase the power density. The proposed converter utilizes three-level Active Neutral Point Clamped (ANPC) topology to reduce the voltage stress in all devices allowing the converter to be used in 800V battery systems. The phase-shift PWM (PSPWM) modulation strategy is proposed for controlling the ANPC half-bridge, this modulation strategy is easy to implement and guarantee the even losses distribution and natural voltage balancing across all switching devices. The operation of the proposed three-level DAHB converter is confirmed by the experimental results.

Keywords – Dual active bridge (DAB), On-board Charger, GaN, bidirectional, multilevel

1. INTRODUCTION

The rise in electrical vehicles (EV) popularity requires battery chargers and power electronics that are reliable, smaller and efficient on the wide operation range of the battery [1]. These performances could be enabled using Gallium Nitride (GaN) devices, with their improved switching characteristics and lower on-resistance [2]. The charging time as well as the whole performances of EVs can be increased by upgrading the high voltage (HV) battery pack from 400 V to 800 V [3]. Nevertheless, the most commonly available and mature GaN transistors are qualified at 650 V [4], which require the use of multilevel topologies in order to address the 800 V applications.

The dual active bridge (DAB) isolated dc-dc topology have been used in various applications, but it has been particularly interesting for EV charging application due to its high efficiency, ease of ZVS, reliability and bidirectional power flow [5] [6]. Furthermore, the DAB topology can be designed for wide voltage range application [7] which is suitable for battery charging applications. The DAB topology is based on two bridges linked through a high frequency AC-link transformer, allowing inherent bidirectional power flow. Advantages and disadvantages of different DAB configurations are presented in [8].

This paper reports the physical implementation of a high-voltage dc-dc converter for automotive application based on 650 V GaN devices.

2. OPERATION PRINCIPLE

2.1. Proposed topology

Multilevel topologies have been used in the last decades in industrial and traction applications as a mean to enable higher power and voltage, the most widely used multilevel topologies are neutral-point-clamped (NPC), flying-capacitor (FC) and T-type topology [9]. FC topology require a complex control, the floating capacitors store high energy, and it requires plenty of voltage sensors in order to ensure the voltage balancing of floating capacitors. T-type topology has minimal component count which is good for power density and efficiency, however, there is high voltage stress on the switching devices rendering it unsuitable for high voltage applications using 650 V devices. On the other hand, NPC topology has no floating capacitors, furthermore, the design is simple, low cost and compact in three-level structure [9]. NPC topology can be further improved using active switches instead of clamping diodes for better efficiency and reliability.

Fig. 1 represents the proposed topology. The proposed three-level DAHB converter is constructed using two three-level ANPC legs, one half-bridge on each side of the transformer. Each half-bridge consists of 6 active devices, and is able to generate a three-level voltage. S_1–S_8 are regular NPC switching devices, while D_1–D_4 are active clamping devices.

Table 1 shows the switching states corresponding to the three level voltage applied to the primary side ($\frac{V_{in}}{2}$, 0 and $-\frac{V_{in}}{2}$). 0 V state can be generated using multiple switching state, hence, the performances of the converter could be optimized using the appropriate zero switching state for each operating point.

TABLE 1. Switching states of a three-level ANPC half-bridge

$S_1/\overline{D_1}$	S_2	S_3	$S_4/\overline{D_2}$	V_p(V)
1	1	0	0	$\frac{V_{in}}{2}$
0	0	1	1	$\frac{V_{in}}{2}$
1	0	1	0	0
0	1	0	1	0
0	1	1	0	0
0	0	1	0	0
0	1	0	0	0

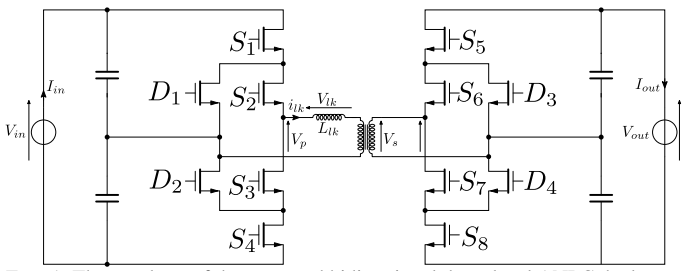

FIG. 1. The topology of the proposed bidirectional three-level ANPC dual active half bridge.

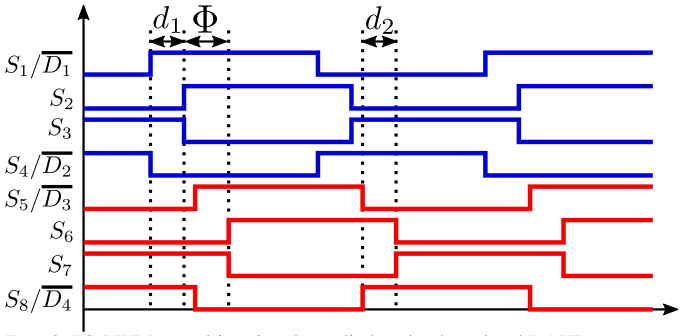

FIG. 2. PS-PWM gate drive signals applied to the three-level DAHB

2.2. *Dual phase shift modulation strategy*

Phase-Shifted Pulse Width Modulation (PS-PWM) is applied to the primary and secondary ANPC half-bridges in order to generate the three-level square voltage. Fig. 2 shows the gate drive signals of the different devices in the proposed converter, all devices switch at 50% duty cycle with a phase shift applied between the outer switches (S_1–S_4 and S_5–S_8) and inner switches (S_2–S_3 and S_6–S_7). The phase shift d_1 is applied to the primary half-bridge, while d_2 is applied to the secondary half-bridge. To simplify the analysis and the design of the proposed converter, d_1 and d_2 are considered equal and are referred to as d_1 in the following. PS-PWM modulation is selected for its multiple advantages such as natural voltage balancing of the different devices, even losses distribution and ease of implementation. The natural voltage balancing is highly desirable as it eliminates the need of using sophisticated and resource-heavy active voltage balancing algorithms.

2.3. *Power flow equation*

Similar to the two-level DAB converter, the power flow of the three-level DAHB converter is controlled by adjusting the phase shift Φ between the two square voltages of the primary and secondary half-bridges. This phase shift creates a voltage across the series inductor, which leads to a power transfer from the leading half-bridge to the lagging half-bridge. The transferred power from the primary side to the secondary side is described by (1), in which P_{out} is the average output power, ω is the switching angular frequency, and n is the turn ratio of the AC-link transformer. This equation is valid only in the case of $d_1 < \Phi < \frac{\pi}{2}$. The value and the direction (direct or reversed) of the transferred power can be controlled by choosing the appropriate combination of d_1 and Φ.

$$P_{out_{3L}} = \frac{n \cdot V_p \cdot V_s}{\omega \cdot L_{lk_{3L}}} \cdot (\Phi - \frac{\Phi^2}{\pi} - \frac{d_1^2}{\pi}) \quad (1)$$

$$P_{out_{2L}} = \frac{n \cdot V_p \cdot V_s}{\omega \cdot L_{lk_{2L}}} \cdot (\Phi - \frac{\Phi^2}{\pi}) \quad (2)$$

If $d_1 = 0°$ in (1), the equation is reduced to the conventional two-level DAB converter equation (2). Furthermore, under the same conditions (same power, frequency and input/output voltages), the ratio between the series inductance of the two-level DAB and three-level DAHB is always less than 1 (3). Thus, the series inductance value is smaller in three-level DAHB converter compared to the two-level DAB converter.

$$R = \frac{L_{lk_{3L}}}{L_{lk_{2L}}} = 1 - \frac{d_1^2}{\pi \cdot (\Phi - \frac{\Phi^2}{\pi})}, \; d_1 < \Phi < \frac{\pi}{2} \quad (3)$$

Fig. 3 shows the different theoretical waveforms of the three-level ANPC DAHB under the condition of $d_1 < \Phi < \frac{\pi}{2}$. This condition can be considered the generalized case [10]. The near-sinusoidal shape of the transformer current contains very few harmonics (THDi) which results in more efficient and smaller magnetics, eventually leading to greater compactness.

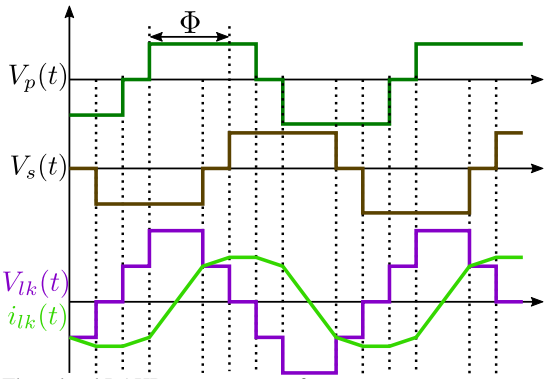

FIG. 3. Three-level DAHB converter waveforms

2.4. *Simulation*

A simulation model is developed using PLECS software to validate the operation of the proposed topology. Fig. 4 shows the operation of the three-level DAHB converter in simulation.

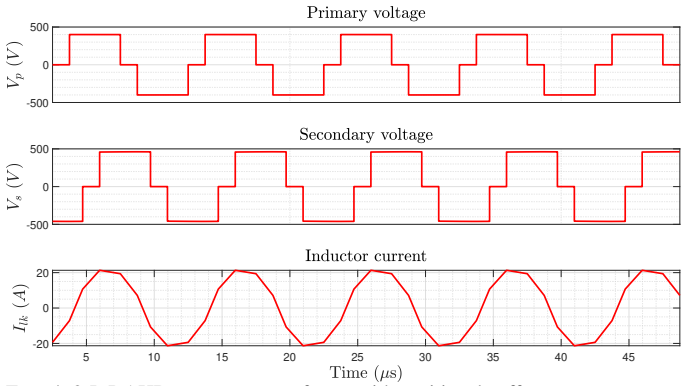

FIG. 4. 3-L DAHB converter waveforms with positive dc offset current.

The model is also able to estimate the efficiency of the converter by calculating the switching and conduction losses of the devices. Switching losses are estimated using extracted switching energies E_{on} and E_{off} from double pulse tests, as presented in Fig. 5. Conduction losses are estimated using the maximum value of $R_{ds,on}$ from the datasheet.

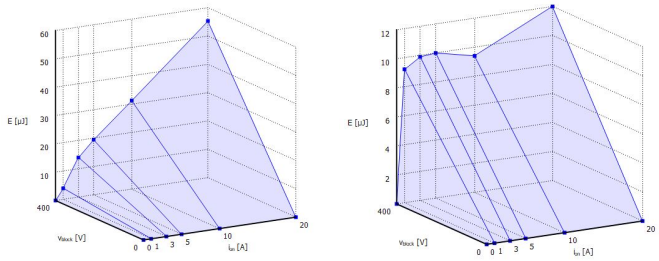

(a) Turn-on switching energies (b) Turn-off switching energies

FIG. 5. Switching energies for different I_{DS} values and V_{DS}=400 V for STMicroelectronics 65mωGaN HEMT device.

The ZVS operation of the proposed topology takes full advantage of the GaN devices because the turn-off losses are 10 time smaller than the turn-on losses for GaN HEMTs.

3. PHYSICAL IMPLEMENTATION

The realized three-level DAHB converter is modular. Each ANPC leg is built with three daughter boards, as seen in Fig. 6. Each daughter board implements a GaN-based two-level half-bridge optimized for very low power loop stray inductance. The daughter boards are implemented using STMicroelectronics 650 V GaN HEMTs with $R_{DS,on}$ of 65 mΩ in a PowerFLAT5x6 package.

The main parameters of the realized prototype are given in Table 2.

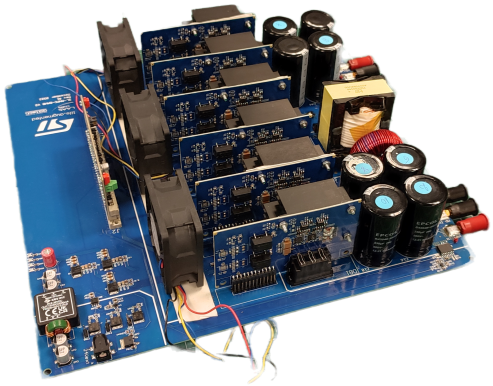

FIG. 6. View of the realized three-level DAHB converter

TABLE 2. Parameters of the three-level DAHB converter

Parameter		Value		
		Min	**Typ.**	**Max**
Input voltage	V_{in}	600V		800V
Output voltage	V_{out}	600V		800V
Rated output power	P_{out}			3.3 kW
transformer turns ration	n_p/n_s		1 :1	
Switching frequency	f_{sw}			500 kHz
Series inductor	L_{lk}		10 µH	

The dual phase shift modulation strategy used to control the power flow of the converter is implemented on STMicroelectronics 32-bit MCU STM32G474 clocked at 170 MHz.

4. EXPERIMENTAL RESULTS

In order to validate the realized converter, the operation is verified using 135mΩ superjunction Si-MOSFETs in PQFN8x8 package. Fig. 7 shows the experimental waveforms of the proposed topology using superjunction Si-MOSFETs for V_{in}=V_{out}=800 V, P_{out}=3.4 kW and f_{sw}=50 kHz. The topology works as intended and as seen in simulations. Furthermore, voltage of the input and output capacitors is balanced and equal to $V_{in}/2$.

Fig. 8 represents the efficiency of the converter using superjunction Si-MOSFETs for switching frequencies of 50 kHz and 100 kHz. The efficiency decreases considerably when increasing the switching frequency, even in ZVS operation. This is due to the big intrinsic capacitors of the Si-MOSFETs which show the limitation of Si-MOSFET technology in high frequency applications.

Fig. 10 shows the efficiency of the converter using STMicroelectronics 65mΩ GaN HEMT device in PowerFLAT5x6 package. The proposed topology achieves the ZVS operation of all switching devices on a wide operation range, thus, the turn-on losses are nonexistent. Furthermore, the turn-off losses are very

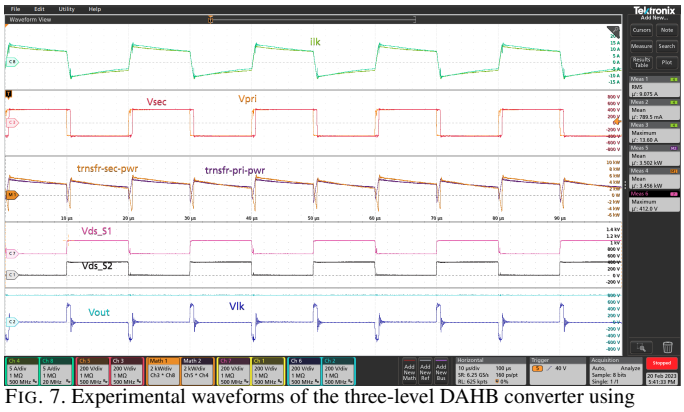

FIG. 7. Experimental waveforms of the three-level DAHB converter using 135mΩ superjunction Si-MOSFET. V_{in}=V_{out}=800 V, P_{out}=3.4 kW, f_{sw}=50 kHz.

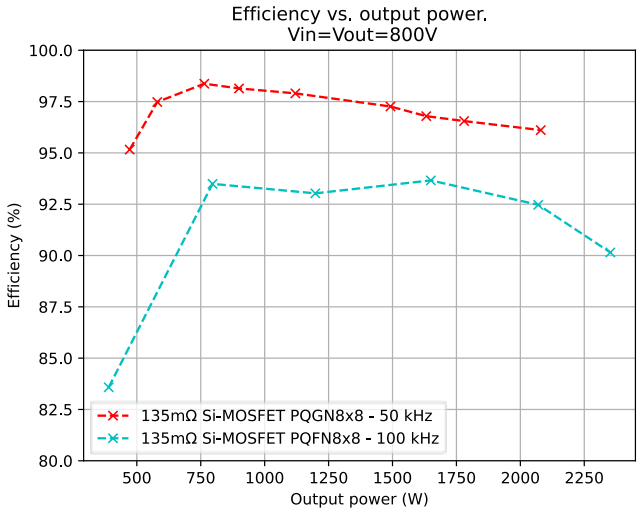

FIG. 8. Efficiency of the proposed converter vs. output power using 135mΩ superjunction Si-MOSFETs.

low for the used GaN HEMT devices as seen in Fig. 5. Hence, The efficiency of the converter is lightly impacted when increasing the frequency from 100 kHz to 400 kHz. Nonetheless, at light loads, the ZVS is lost, so the efficiency is low at light loads. Moreover, the temperature increase ΔT of S_1 device is 10°C for switching frequency between 50 kHz and 400 kHz which proves the low switching losses of the devices in the proposed topology.

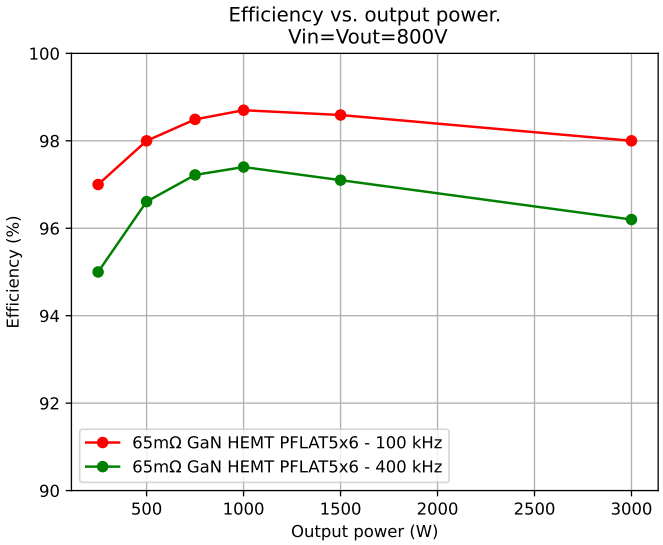

FIG. 9. Efficiency of the proposed converter vs. output power using 65mΩ GaN HEMT.

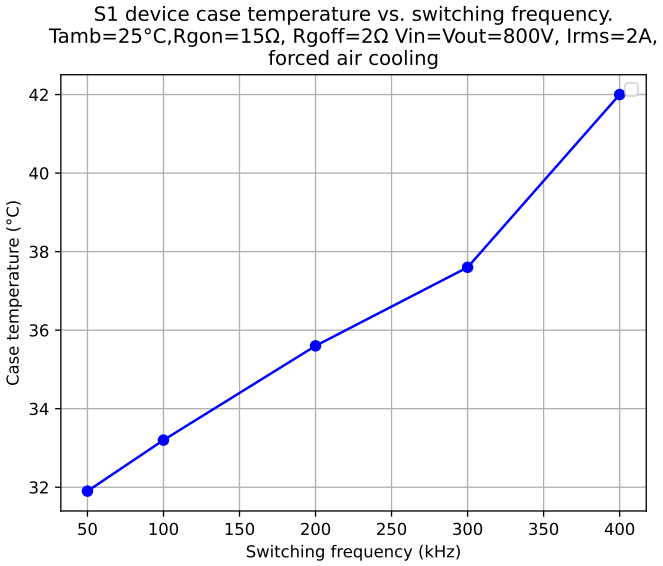

FIG. 10. Case temperature of S_1 device for V_{out}=V_{in}=800 V and P_{out}=1.6kW and different switching frequencies.

Fig. 11 shows the key waveforms of the converter at 400 kHz, it can be seen that even at the high switching frequency operation, the waveforms stay clean and without overshoot or oscillations even at high dv/dt and di/dt. Thus, the layout of the board present minimum stray inductance.

5. CONCLUSION

This paper has presented the design and realization of a GaN-based three-level DAHB converter for high voltage automotive applications. The converter works under dual-phase shift modulation and features fast and low on-state resistance GaN devices. The converter design and its control have been verified on a physical 3.3 kW prototype in both 100 and 400 kHz.

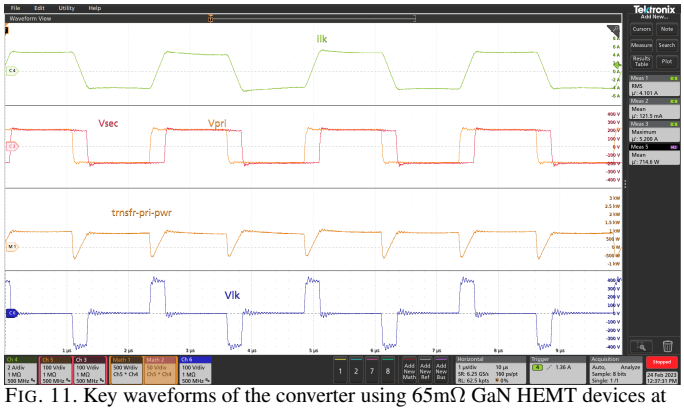

FIG. 11. Key waveforms of the converter using 65mΩ GaN HEMT devices at 400 kHz.

Future work will focus on implementing a feedback control loop and increasing the power of the converter using lower on-state resistance GaN devices.

6. REFERENCES

[1] M. Safayatullah, M. T. Elrais, S. Ghosh, R. Rezaii and I. Batarseh, "A Comprehensive Review of Power Converter Topologies and Control Methods for Electric Vehicle Fast Charging Applications," in IEEE Access, vol. 10, pp. 40753-40793, 2022, doi : 10.1109/ACCESS.2022.3166935.

[2] J. Millán, P. Godignon, X. Perpiñà, A. Pérez-Tomás and J. Rebollo, "A Survey of Wide Bandgap Power Semiconductor Devices," in IEEE Transactions on Power Electronics, vol. 29, no. 5, pp. 2155-2163, May 2014, doi : 10.1109/TPEL.2013.2268900.

[3] C. Jung, "Power Up with 800-V Systems : The benefits of upgrading voltage power for battery-electric passenger vehicles," in IEEE Electrification Magazine, vol. 5, no. 1, pp. 53-58, March 2017, doi : 10.1109/MELE.2016.2644560.

[4] S. Chowdhury et al., "650 V Highly Reliable GaN HEMTs on Si Substrates over multiple generations : Expanding usage of a mature 150 mm Si Foundry," 2019 30th Annual SEMI Advanced Semiconductor Manufacturing Conference (ASMC), Saratoga Springs, NY, USA, 2019, pp. 1-5, doi : 10.1109/ASMC.2019.8791814.

[5] P. He and A. Khaligh, "Comprehensive Analyses and Comparison of 1 kW Isolated DC–DC Converters for Bidirectional EV Charging Systems," in IEEE Transactions on Transportation Electrification, vol. 3, no. 1, pp. 147-156, March 2017, doi : 10.1109/TTE.2016.2630927.

[6] B. Zhao, Q. Song, W. Liu and Y. Sun, "Overview of Dual-Active-Bridge Isolated Bidirectional DC–DC Converter for High-Frequency-Link Power-Conversion System," in IEEE Transactions on Power Electronics, vol. 29, no. 8, pp. 4091-4106, Aug. 2014, doi : 10.1109/TPEL.2013.2289913.

[7] P. A. M. Bezerra, F. Krismer, R. M. Burkart and J. W. Kolar, "Bidirectional isolated non-resonant DAB DC-DC converter for ultra-wide input voltage range applications," 2014 International Power Electronics and Application Conference and Exposition, Shanghai, China, 2014, pp. 1038-1044, doi : 10.1109/PEAC.2014.7038003.

[8] H. Higa, S. Takuma, K. Orikawa and J. -i. Itoh, "Dual active bridge DC-DC converter using both full and half bridge topologies to achieve high efficiency for wide load," 2015 IEEE Energy Conversion Congress and Exposition (ECCE), Montreal, QC, Canada, 2015, pp. 6344-6351, doi : 10.1109/ECCE.2015.7310549.

[9] A. Poorfakhraei, M. Narimani and A. Emadi, "A Review of Multilevel Inverter Topologies in Electric Vehicles : Current Status and Future Trends," in IEEE Open Journal of Power Electronics, vol. 2, pp. 155-170, 2021, doi : 10.1109/OJPEL.2021.3063550.

[10] Moonem, M. A., C. L. Pechacek, R. Hernandez, and H. Krishnaswami. 2015. "Analysis of a Multilevel Dual Active Bridge (ML-DAB) DC-DC Converter Using Symmetric Modulation" Electronics 4, no. 2 : 239-260. https ://doi.org/10.3390/electronics4020239